



This is a repository copy of *Evaluation of catheter-induced tribological damage to porcine aorta using infra-red spectroscopy*.

White Rose Research Online URL for this paper:  
<http://eprints.whiterose.ac.uk/105867/>

Version: Accepted Version

---

**Article:**

Dellimore, K.H.J., Mank, A.J.G., Wojnowski, J. et al. (2 more authors) (2016) Evaluation of catheter-induced tribological damage to porcine aorta using infra-red spectroscopy. *Biotribology*, 7. pp. 11-21.

<https://doi.org/10.1016/j.biotri.2016.07.002>

---

Article available under the terms of the CC-BY-NC-ND licence  
(<https://creativecommons.org/licenses/by-nc-nd/4.0/>)

**Reuse**

This article is distributed under the terms of the Creative Commons Attribution-NonCommercial-NoDerivs (CC BY-NC-ND) licence. This licence only allows you to download this work and share it with others as long as you credit the authors, but you can't change the article in any way or use it commercially. More information and the full terms of the licence here: <https://creativecommons.org/licenses/>

**Takedown**

If you consider content in White Rose Research Online to be in breach of UK law, please notify us by emailing [eprints@whiterose.ac.uk](mailto:eprints@whiterose.ac.uk) including the URL of the record and the reason for the withdrawal request.



[eprints@whiterose.ac.uk](mailto:eprints@whiterose.ac.uk)  
<https://eprints.whiterose.ac.uk/>

# Evaluation of catheter-induced tribological damage to porcine aorta using infra-red spectroscopy

Kiran HJ Dellimore<sup>a</sup>, Arjan JG Mank<sup>a</sup> Jacek Wojnowski<sup>b</sup>, Chris Noble<sup>c</sup>, Steven E Franklin<sup>a,d</sup>

<sup>a</sup>Philips Research, Eindhoven, the Netherlands; <sup>b</sup>West Pomeranian University of Technology, Faculty of Mechanical Engineering and Mechatronics, Institute of Materials Engineering, 19 Piast Avenue, Szczecin, Poland; <sup>c</sup>University of Sheffield, CISTIB Centre for Computational Imaging and Simulation Technologies in Biomedicine, Department of Mechanical Engineering, Sheffield, UK; <sup>d</sup>University of Sheffield, Leonardo Tribology Centre, Sheffield, UK.

## Corresponding Author:

Steve Franklin

Philips Research,  
High Tech Campus 4, 5656 AE,  
Eindhoven, the Netherlands

**Tel:** +31 (0)6 226 84346

**Email:** [s.e.franklin@philips.com](mailto:s.e.franklin@philips.com)

## Abstract:

Studies were carried out to assess the potential of attenuated total internal reflection Fourier transform infrared (ATR)-FTIR spectroscopy as a tool for evaluating mechanical-tribological damage to the blood vessel wall occurring during simulated endovascular catheterization on fresh ex-vivo porcine aortic tissue. It is envisaged that this method could be used in laboratory tests to quantitatively compare catheters or catheterization approaches with regard to their effect on damage to the aorta wall.

Tribological damage was induced on the tissue. Obvious changes were visible in the FTIR spectra as well as the friction coefficient as a function of increasing damage. In particular, the spectral changes due to damage to the outermost layer of the tissue were significant, provided appropriate sample conditioning was performed. These changes, which correlated with a reduction in friction coefficient, can be attributed to the removal of successive layers of tissue as a result of a wear process. In conclusion, FTIR spectroscopy was found to be a reliable and effective measurement technique for quantifying catheter-induced tissue

damage, allowing very repeatable spectra to be obtained from the tissue up to 36 hours after excision with no major spectral changes observed during this time frame due to tissue age.

**Keywords:** endovascular catheters; ATR-FTIR spectroscopy; vascular trauma; tissue damage characterization; catheter-induced damage; mechanical damage quantification.

## 1. INTRODUCTION

Cardiovascular system disease is one of the main health problems and the leading cause of death in European countries. Annually more people die due to cardiovascular failure than from chronic respiratory tract diseases and cancer [1]. Endovascular catheterization is among the key interventions used to treat individuals suffering from cardiovascular diseases such as aortic valve stenosis, coronary heart disease, heart block and abdominal aortic aneurysms [2]. Every year more than 200 million endovascular catheters are used during endovascular catheterization procedures (ECP) [3]. Complications during ECP can have different origins; however, the most important source of complications, including arterial spasm, cardiac tamponade, hematoma and vascular trauma [4-6], is the mechanical-tribological interaction between the endovascular catheter and the blood vessel wall [7]. Therefore, a deeper understanding of the tissue damage process is needed to study this interaction in detail to look for opportunities to reduce or minimize the aforementioned complications. This in turn will yield faster recovery from surgery, shorter hospital stays, fewer readmissions and lower mortality during ECP.

Several methods have been previously used or may be potentially used to characterize damage to biological tissue arising as a result of the rubbing action of a catheter on its inner surface. These can be broadly classified into two main categories: destructive and non-destructive methods. Destructive tissue damage characterization methods are suitable only for ex-vivo tissue testing and include histology (with chemical or cryogenic tissue fixation) [8], optical (light) microscopy [9], scanning electron microscopy (SEM) [10-11], and environmental SEM [12-13]. Non-destructive methods are more suited for in vivo tissue testing and include techniques such as optical coherence tomography (OCT) [14-15], ultrasound [16], white light interferometry [17], Raman spectroscopy [18-19], and infrared (IR) spectroscopy [20-22]. Of these approaches the most promising for further exploration are the methods based on Raman and IR spectroscopy. However, despite its advantages, Raman spectroscopy has limitations which make it less suitable for tissue damage characterization due to catheterization. In particular, Raman spectroscopy requires the use of microscopy to obtain sufficient signal. This makes it very sensitive to small inhomogeneities that are common in actual tissue. The scattering nature of tissue helps to limit the effect, but in turn reduces the specificity at the surface (where most catheter linked

damage is expected to occur). Finally, the largest variations expected in tissue are linked to polar bonds, for which Raman spectroscopy is inherently less sensitive than IR spectroscopy.

As a result IR spectroscopy is considered more promising since this technique has a high identification power and can be made surface selective. It has the potential to detect very subtle changes in the biochemical structure of tissue linked to mechanical-tribological damage caused by catheterization, and may be used in vivo.

The main aim of this work is therefore to provide a basis for a spectroscopic method that can be used for in vitro laboratory analysis to compare the damage to the blood vessel wall caused by different catheter designs, materials or catheterization approaches. This should provide the necessary starting point for the optimization of catheter-tissue interaction to limit damage during actual procedures.

## **2. BACKGROUND**

### **2.1 Blood Vessel Wall Structure**

In order to make sense of spectroscopic differences that are observed as a function of the level of tissue damage encountered it is important to first have a basic understanding of biological tissue, which by its nature is a very complicated, highly variable and inhomogeneous material. To do this it is useful to take a closer look at the actual structure of the blood vessel wall, using aortic tissue as a reference due to its ubiquity in many ECP.

Aortic tissue, in particular, has a strongly stratified structure, which is divided into three layers- the intima, media and adventitia (as encountered by a catheter during arterial perforation from the inside); each of which serves a well-defined purpose:

1. The Intima - is a larger structure composed of three constituents, which together protect the artery wall from the inside and provide reduced friction between the vessel inner lining and blood flowing through the lumen of the artery. Its biochemical composition consists mostly of carbohydrates and proteins. The three constituents of the intima include the following:
  - i. *Glycocalyx* – a negatively charged layer composed of glycoproteins and proteoglycans, performing a wide variety of critical functions in the fluid environment, such as the mechano-transduction of shear stress, exclusion of red blood cells from the endothelial cell (EC) monolayer, modulation of leukocyte attachment and rolling, and inhibition of platelet adhesion. The glycocalyx is roughly 0.5-3.0  $\mu\text{m}$  thick [23].

- ii. *Endothelial cells* – a monolayer of cells, approximately 0.2  $\mu\text{m}$  thick [23].
  - iii. *Internal lamina* – a layer of elastic tissue that separates the intima from the media.
2. The Media - is, volumetrically, the largest layer in the aorta wall. It is a composite layer that is made up of smooth muscle cells and elastic tissue (i.e., layers of crisscrossing elastin strands and collagen fibers embedded in the intercellular matrix). Its main purpose is to allow arterial deformation and recovery (i.e., dilation and contraction) during blood flow. In a biochemical sense the media consists mainly of proteins, carbohydrates, phosphates and to a small extent, lipids.
  3. The Adventitia – consists of thick bundles of irregularly distributed collagen fibers in a matrix of fibroblasts, smooth muscle cells, and connective tissue. It provides mechanical resistance to the pulsating blood pressure. Biochemically the adventitia is composed mainly of proteins, phosphates and lipids.

The breakdown of the biological structure, main constituents and biochemical makeup of the arterial wall of the aorta are summarized below in **Table 1**.

**Table 1 Biological structure, main constituents and biochemical makeup of the arterial wall of the aorta.**

	<b>Intima</b>	<b>Media</b>	<b>Adventitia</b>
<b>Structure</b>	Glycocalyx Endothelial cells Internal lamina	SMC - rich in proteoglycans Aligned (mainly) collagen and elastin fibers - rich in proteoglycans External elastic lamina Note: SMC, collagen and elastin content may vary depending on the distance from the heart	Thick bundles of helically arranged collagen (forming fibrous tissue) Fibroblasts Connective tissue
<b>Main constituents</b>	Glycocalyx Monolayer of endothelial cells Connective tissue Basal lamina (mesh-like collagen, adhesion molecules, fibronectin and laminin)	Smooth muscle cells Connective tissue Polysaccharide substances Elastic fibers External elastic lamina	Bundles of collagen fibrils Fibroblasts Few elastic fibers Smooth muscle cells

Chemical make-up	Glycocalyx glued with polysaccharides Collagen Adhesion molecules (proteins) Fibronectin (HMW glycoprotein) Laminin (protein)	Smooth muscle cells (Myosin, Actin) [Fibroblasts-cells, Collagen-proteins, Proteoglycans-glycosylated proteins, Adipocytes-fat cells Polysaccharides (Carbohydrates) Collagen Elastin	Collagen Fibroblasts – cells Elastin Smooth muscle cells
Generalized chemical make-up	Carbohydrates Proteins	Proteins, Lipids, DNA, Phosphates Carbohydrates	Proteins, Lipids, DNA, Phosphates

Abbreviation(s): DNA = deoxyribonucleic acid, HMW = high molecular weight, SMC = smooth muscle cells.

## 2.2 Definition of Mechanical Tissue Damage Levels

When considering mechanical damage to the blood vessel wall occurring during an ECP, it is important to first consider how extensive the tissue damage needs to be in order to be deemed serious. Although this likely varies greatly depending on the state of health of the patient undergoing catheterization, type of blood vessel, age, etc., a benchmark is needed in order to establish a suitable baseline for the observable spectroscopic differences.

A recent study by Sobolewski and El Fray may provide a useful starting point [24]. They point out that the use of a balloon catheter to denude an artery segment has long been utilized as a model of arterial injury and intimal thickening, and explain the mechanisms involved in the healing of the arterial wall after damage. Following arterial injury, platelets and leukocytes are rapidly recruited to the injury site, and within twenty-four hours, smooth muscle cells (SMC) from the media layer begin to replicate, due to a combination of growth factor release from injured SMC, access to blood-born growth factors, and the absence of inhibitory endothelial cell signaling, including nitric oxide. This initial response to injury is then followed by additional SMC migration and proliferation, along with the deposition of extracellular matrix proteins, ultimately leading to the formation of neointima and a stenosis (i.e., narrowing) of the artery.

According to the Sobolewski and El Fray [24], the critical moment in mechanical damaging of the artery wall occurs when the thin intima layer is removed, either by scraping, friction (i.e., abrasion or rubbing), or exposing of the media layer. Based on this finding, in the current

study “acceptable” damage is defined as mechanical injury to the arterial wall which does not result in a change in the porcine aortic spectrum from one typical for that of the intima to one typical for that of the media. Any other observable spectrum changes are considered “serious” or “unacceptable” damage, independent of whether they were caused by scraping, abrasion, dissection or perforation of the artery wall.

### **2.3 Spectroscopic Implications of Mechanical Tissue Damage**

From a biological point of view it is known what to expect when mechanical damage is inflicted upon the aortic tissue on the basis of knowledge of the main chemical constituents in the tissue which can be summarized as follows [25-26]:

- Proteins that can be found in the media, building collagen and elastin fibers [27].
- Phosphates that, with or without lipids, are building cell plasma membranes or DNA and RNA macromolecules [28].
- Carbohydrates that are present in the tissue in the form of free glycogen (living organism energy source [27]) and in other forms such as the glycocalyx layer in the intima [23].

The spectral signatures for these various tissue constituents are given below, with the regions arbitrarily defined for convenience in the current study [20, 22-23, 25-33]:

- Region I – Spectral peaks originate mainly from carbohydrates, and to a lesser extent from proteins and phosphates ( $1130\text{-}1000\text{ cm}^{-1}$ )
- Region II – Spectral peaks originate mostly from carbohydrates and to a lesser extent from proteins ( $1180\text{-}1130\text{ cm}^{-1}$ )
- Region III – Spectral peaks originate mainly from proteins, and to a lesser extent from phosphates and carbohydrates ( $1360\text{-}1180\text{ cm}^{-1}$ )
- Region IV – Spectral peaks originate from proteins and carbohydrates ( $1430\text{-}1360\text{ cm}^{-1}$ )
- Region V – Spectral peaks originate from proteins ( $1480\text{-}1430\text{ cm}^{-1}$ )

When changing between the three main tissue layers, characteristic spectral changes are expected. However, there are large discrepancies in the literature over the spectral changes in the above-defined regions which occur due to damage [30, 34-38]. This is likely attributable to the fact that this research involves heterogeneous, live biological tissue and samples extracted from different body locations under various conditions which may have introduced spectral differences between the observations reported in the literature. In principle, the best approach is to use one type of material and a well-defined sample preparation. Tracking the changes in the infrared spectra while introducing progressive

damage should allow the layers to be distinguished and permit characterization of three types of aortic tissue damage:

1. Damage within the intima layer, e.g., denudation of the artery wall due to catheter friction.
2. Damage extending as far as the media, which is predominantly collagen, e.g., dissection of the arterial wall by the catheter.
3. Damage extending as far as the adventitia (stroma, connective tissue), e.g., arterial wall perforation by the catheter tip.

To address the inconsistency in the spectral data from literature, the development of a spectroscopic method for the assessment of vascular damage caused by mechanical interaction with a catheter was conducted by performing a systematic, experimental investigation divided into two parts. The first part of the experimental investigation focused on qualitative analysis to ascertain what spectral differences could be observed when significant damage is inflicted upon the aortic tissue, while in the second part the possibility of characterizing more controlled and more realistic damage caused by a catheter tip was investigated.

### **3. METHODS**

The development of a spectroscopic method for tissue damage characterization was conducted in two parts, a qualitative exploration of the ability of ATR-FTIR to discriminate between clearly damaged and undamaged tissue, followed by an investigation involving more controlled tissue damage conditions using actual catheter tips. It is important to note here that there are several possible approaches that could be used to damage the aortic wall. The two most relevant to catheterization are incisions and friction (i.e., abrasion) [47]. In this study emphasis is placed on abrasion as it produces more even (i.e., uniform) mechanical damage of the arterial wall structure. Due to ethical and practical reasons all experiments were performed using ex-vivo porcine aortic tissue (sourced from Hemolab BV in Eindhoven, the Netherlands, an ethical tissue supplier). The tissue was harvested from Dutch, female, Landrace hybrid piglets, with an average age of 6 months, which were humanely slaughtered for human consumption. The protocols at the slaughterhouse and in the laboratory followed European Commission regulations 1774/2002 regarding the use of slaughterhouse animal material for diagnosis and research, supervised by the Dutch Ministry of Agriculture, Nature and Food Quality and are approved by the associated legal authorities of animal welfare (Food and Consumer Product Safety Authority).

Ethical approval for this study was obtained from the Philips Research Internal Committee for Biological Experiments.

### **3.1 Sample preparation**

The following sample preparation protocol was used for all tests:

1. A sterile scalpel was used to cut the fresh ex-vivo porcine aorta into a 2.5 cm by 2.5 cm square test specimen, taking care not to damage the interior tissue structure.
2. The test specimen was then thoroughly washed in warm (37°C) phosphate buffered saline (PBS) solution.
3. The test specimen was placed in a 10 ml plastic petri dish and immersed in 5 ml of PBS.
4. The container was covered and the tissue specimen refrigerated overnight at 4°C.

### **3.2 Tissue damage / tribological test protocol**

Different protocols were used to damage the tissue in the first (qualitative assessment) and second (controlled tissue damage) experiments.

#### **3.2.1 Qualitative assessment**

A simple protocol was used in the initial experiments, which were aimed at investigating whether any spectral changes could be observed as a result of clearly damaging the tissue (based on visual inspection):

1. The tissue specimen was removed from the refrigerator and allowed to equilibrate to room temperature for 30 minutes.
2. Two methods were used to damage the tissue specimen:
  - a. Soft brush: for milder abrasion conditions a Nylon 6/12 brush intended for personal skin care was used (Philips Visapure Model SC5275/10, Philips BV, Eindhoven, the Netherlands). The device was used at the “slow rotating/vibrating” setting ( $180 \pm 27$  rpm,  $80 \pm 8$  Hz vibration with 5—300  $\mu$ m amplitude) and applied to the tissue with a force of  $10 \pm 4$  N.
  - b. Hard brush: for more severe abrasive conditions a Nylon bristle brush intended for hobby purposes was used (Dremel 3000, Robert Bosch Tool Corporation, Mount Prospect, IL, USA). This device was used at a rotation speed of 100 rpm and applied to the tissue with a force of  $20 \pm 5$  N.

The soft brush was used to inflict limited damage to the tissue specimen in a gradual manner. This was accomplished by pressing the rotating brush against the tissue specimen for a prescribed period of time, while taking care not to handle the tissue too much. Progressive abrasion of the tissue with the soft brush was achieved in increments of 60 or 120 s until a total of 900 s of abrasion had been achieved.

The hard brush was used to remove tissue material rapidly to a level where visual inspection clearly showed removal of the outer tissue layer. The specimen was abraded with the hard brush for a maximum of 15 s.

### 3.2.2 Controlled tissue damage testing

In the second part of the study the tissue damage protocol was refined in order to achieve greater control over the level of damage applied to the tissue. Several key differences were implemented:

1. A custom-made tissue holder was fabricated to secure the tissue (**Figure 1a**). The tissue holder enabled the ex-vivo porcine aorta tissue specimen to be stretched laterally and to be held in place reliably during controlled damage testing.
2. A UMT multi-specimen test system from CETR-Bruker, equipped with a DFM-2-0966 force sensor (range = 0.2 N – 20.0 N), (**Figure 1b**) was used to apply a controlled normal force to a catheter tip probe that was subsequently rubbed over the tissue specimen at a defined incidence angle and controlled velocity over a preset rubbing distance. Two types of catheter probes were tested, representing two different levels of stiffness at the catheter tip (**Figure 2a and 2b**). Both probes were 2.3mm in diameter (7 French), 8cm long and made from polyether block amide (PEBAX) copolymer:
  - a. *Tip 1*: tapered tip made from PEBAX 3533 ( $\approx$  hardness 35 Shore D) with shaft made from PEBAX 5533 ( $\approx$  hardness 55 Shore D).
  - b. *Tip 2*: high stiffness tapered tip made from PEBAX 3533 ( $\approx$  hardness 35 Shore D), stiffened by the addition of steel wire inside the lumen, with shaft made from PEBAX 3533 ( $\approx$  hardness 35 Shore D).
3. A custom-built catheter tip head holder was developed to enable the catheter tips to be oriented at specific acute incidence angles relative to the tissue specimen, in order to more closely simulate in vivo catheter-blood vessel contact conditions (**Figure 2c**).
4. A custom-built fluid bath was developed to enable the tissue to be soaked in PBS solution during the test (**Figure 2d**).

The protocol used for the controlled damage tests was as follows:

1. The tissue specimen was removed from the refrigerator, secured in the custom-built tissue holder in the PBS fluid bath and then allowed to equilibrate to room temperature for 30 minutes.

2. The tissue specimen was damaged using the UMT equipped with one of the two catheter tips (after mounting in the custom-built catheter tip holder). The catheter tips were oriented at a 45° angle to the tissue specimen and rubbed at a speed of 1 mm/s against the tissue at a prescribed and force-feedback controlled normal force of 0.2 N over a distance of 20 mm during each pass. Each pass was unidirectional and performed on exactly the same location on the tissue. When necessary, to avoid drying out of the tissue, a pipette was used to add additional PBS solution to the catheter-tissue contact during testing. The normal and tangential forces were recorded during the test, which allowed calculation of the coefficient of friction (COF). The applied normal force was chosen to be within the range of catheter contact forces reported in the literature for various ECP [48-51]. To simulate different damage levels the number of unidirectional passes was varied: 1 pass simulates catheter insertion into the aorta, 5 passes simulates a moderately complex ECP with catheter manipulation, and 10 passes simulates a very complex ECP. In the case of catheter tip 1 the number of unidirectional passes was varied, with 1, 5 and 10 passes applied (experiments 1-3). In these cases the length of free catheter tip extending out of the custom-built catheter tip holder was fixed at 20 mm. For catheter tip 2, 1 and 10 passes were performed with a 20-mm free catheter tip length (experiments 4-5). In experiment 6, 10 passes were also performed using catheter tip 2 but with a shorter (10 mm) free catheter tip length. In this way the catheter tip stiffness and thus the stress acting on the tissue was further increased.

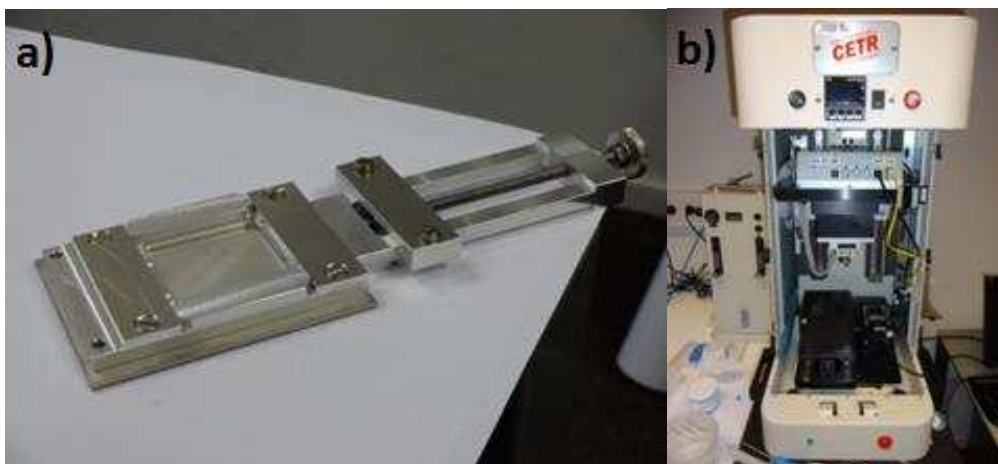


**Figure 1. (a) Photographs of: (a) the custom-built tissue holder and (b) the applied UMT universal tribological test system.**

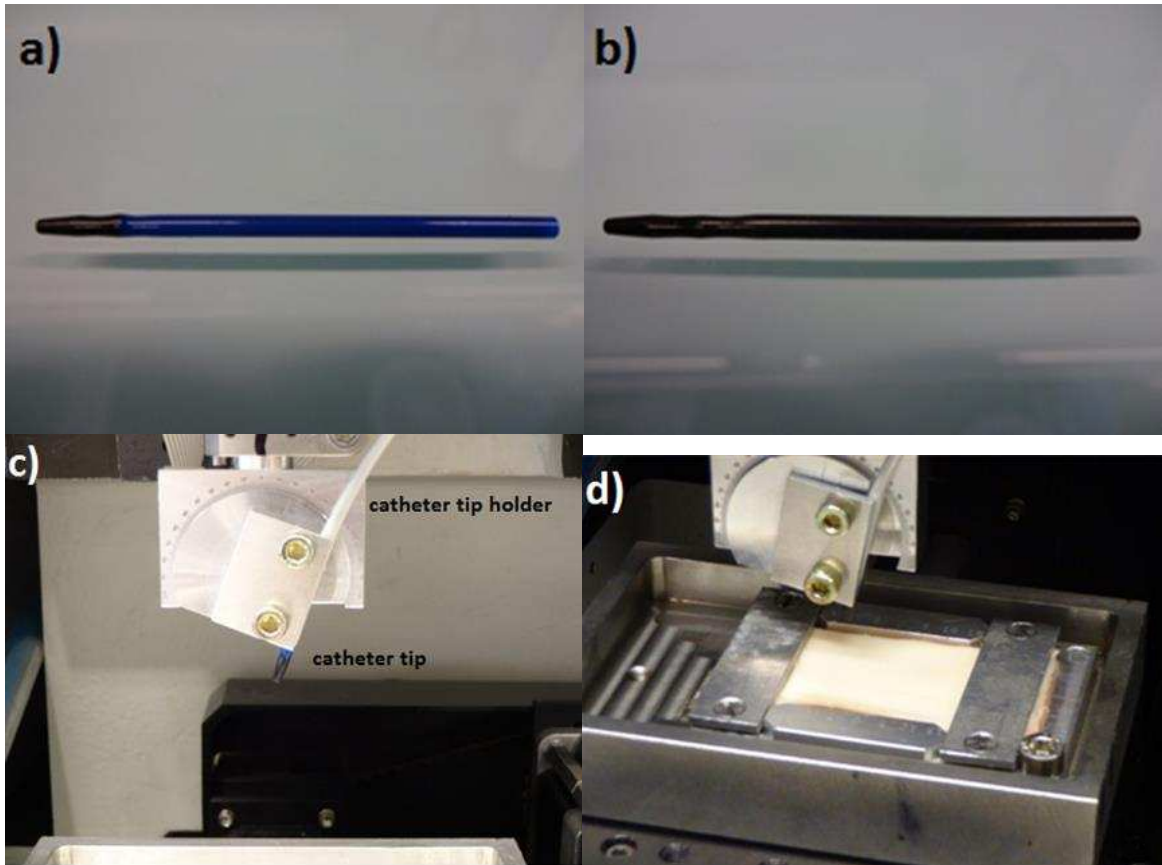


**Figure 2. Photograph of the probes used to inflict controlled damage to the ex-vivo porcine aortic tissue: (a) PEBAX S5533 T3355, (b) PEBAX S3355 T3355. Photographs of the custom-built catheter tip holder: (c) mounted in the UMT and (d) fluid bath and setup for a test on ex-vivo porcine aortic tissue.**

### 3.3 FTIR Measurement

#### 3.3.1 FTIR technique

Fourier-transform IR (FTIR) spectroscopy is based on the direct absorption of IR radiation and it therefore has significantly higher signal intensity than other spectroscopic techniques such as Raman, which involves inelastic light scattering. However, in conventional FTIR (transmission) analysis water produces strong interference as it absorbs a large portion of the radiation. This makes the technique less suitable for biological materials unless special measures are applied. When attenuated total internal reflection (ATR)-IR spectroscopy is used, the presence of water does not have to be limiting [39]. In this approach, the IR beam passes through an IR-transparent crystal in such a way that it reflects at least once at the internal surface in contact with the sample (**Figure 3a and 3b**). The evanescent wave of this reflection extends into the sample and can interact with the material over a short distance. Added advantages of the ATR-FTIR approach are that it requires little sample preparation and the sampling depth is very limited with only the top few micrometers of the surface examined, which is ideal for the analysis of the effect of catheter abrasion on tissue.

Consequently, ATR-FTIR spectroscopy is applied here as the spectroscopic method of choice to assess mechanical damage inflicted on the tissue during catheterization.

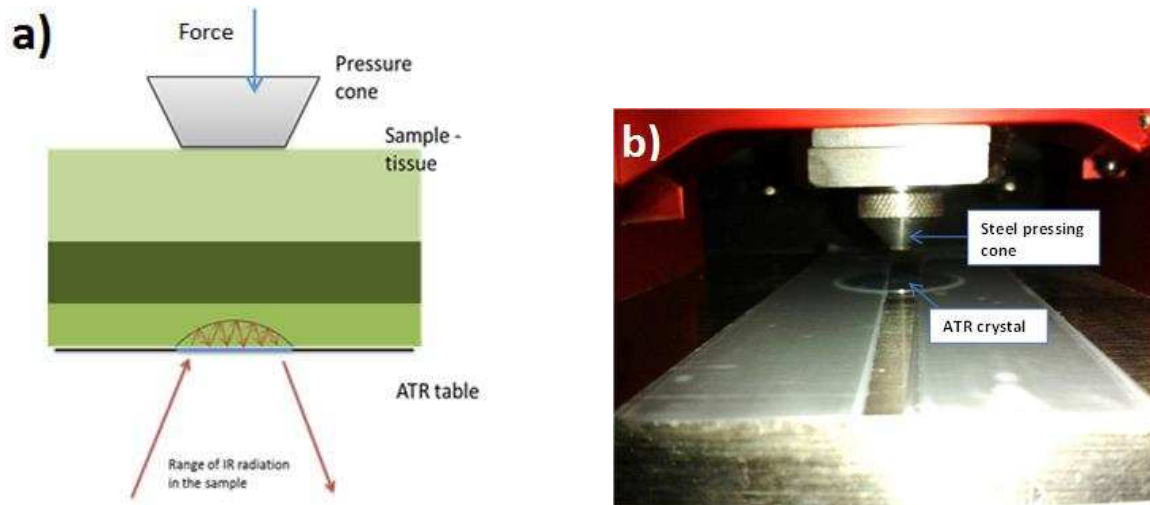


**Figure 3. (a) Schematic illustration showing the sampling approach with attenuated total internal reflection (ATR)-FTIR for the characterization of vascular damage due to catheterization. (b) Photograph of the ATR focusing element with a steel pressure cone and diamond crystal.**

The instrument used in all experiments was a Thermo Nicolet Nexus IR spectrometer with a Specac Golden Gate ATR and MCT detector. The following settings were applied in the measurement setup:

- Crystal material: diamond
- Detector selection in OMNIC program: DTGS 4 cm<sup>-1</sup>
- Wavenumber range analyzed: 4000-650 cm<sup>-1</sup>
- Number of scans: variable (in most cases 192 scans were acquired)
- Resolution: 4 cm<sup>-1</sup>

In order to quantitatively analyze tissue damage it is necessary to have precise knowledge of the ATR-FTIR sampled volume. The exact sampled volume is determined by the radiation wavelength, the angle of incidence and the refraction index of the ATR crystal and the medium being probed [40-41].

Assuming an angle of incidence of 45° and the IR energy generally used in tissue characterization (with most important absorption features between 1800 cm<sup>-1</sup> and 900 cm<sup>-1</sup>), relative 'penetration depth' values can be estimated. According to the literature  $d_p$  can be estimated using the following equation:

$$d_p = \frac{\lambda}{2\pi n_1 [\sin^2 \theta - (n_2/n_1)^2]^{1/2}} \quad (1)$$

where  $\lambda$  is the wavelength (nm),  $n_1$  is the refractive index of the crystal,  $n_2$  is the refractive index of the sample, and  $\theta$  is the angle of incidence [42]. Taking the crystal material into consideration (diamond with  $n_1 = 2.4$ ) [43], average refractive indices  $n_2$  for various tissue types can be found in the literature (**Table 2**).

**Table 2 Values of the refractive index for human and animal tissue.**

Tissue layer	Tissue	$\lambda$ (nm)	Refractive index
Intima	Human arterial tissue	456-1064	1.390 [44]
	Human carotid artery	--	1.352 [45]
Media	Human arterial tissue	456-1064	1.380 [44]
	Human carotid artery	--	1.382 [45]
Adventitia	Human arterial tissue	456-1064	1.360 [44]
	Human carotid artery	--	-- [45]
Muscle	Bovine muscle	592	1.382 [46]

Abbreviation(s):  $\lambda$  = wavelength. Minimum and maximum refractive index values are 1.352 and 1.390.

Substitution of these values into Eq. (1) yielded estimates of the relative ‘penetration depth.’ For the experiments performed in the current study a summary of the values of the average ‘penetration depth’ is provided below in **Table 3**.

**Table 3 Average calculated values of ‘penetration depth’ for the experiments conducted in this study.**

	Estimated $d_p$ ( $\mu\text{m}$ )
Min	2.58
Max	5.45
Average	3.71
Std. dev.	0.12

Abbreviation(s):  $d_p$  = penetration depth

Although these differences may appear large, the contrast is mainly wavelength-dependent as the refractive index of the various layers is very similar. Therefore, differences in the sampled volume due to the degree of damage are not expected to be a concern. Signal from water outside the tissue is limited due to the pressure exerted during analysis (to enable sufficient contact between the tissue and crystal).

### 3.3.2 FTIR analysis protocol

For the initial qualitative assessment of spectral changes due to tissue damage, the damaged specimen was placed in the ATR-FTIR setup for spectroscopic analysis immediately following the damage test. The pressure applied to the ATR pressure cone on the specimen was then adjusted using the 'live mode' so that the absorption level was the same in all tests (i.e., to ensure repeatability and consistency in the ATR-FTIR measurements). Care was taken to ensure that mechanical damage to the tissue, due to the contact pressure between the steel pressing cone and the ATR crystal, was minimized. After a short stabilization period of about 5 s, FTIR spectroscopic analysis was performed over a fixed integration time of typically 237 s (192 scans).

A more refined procedure was followed for the controlled tissue damage experiments:

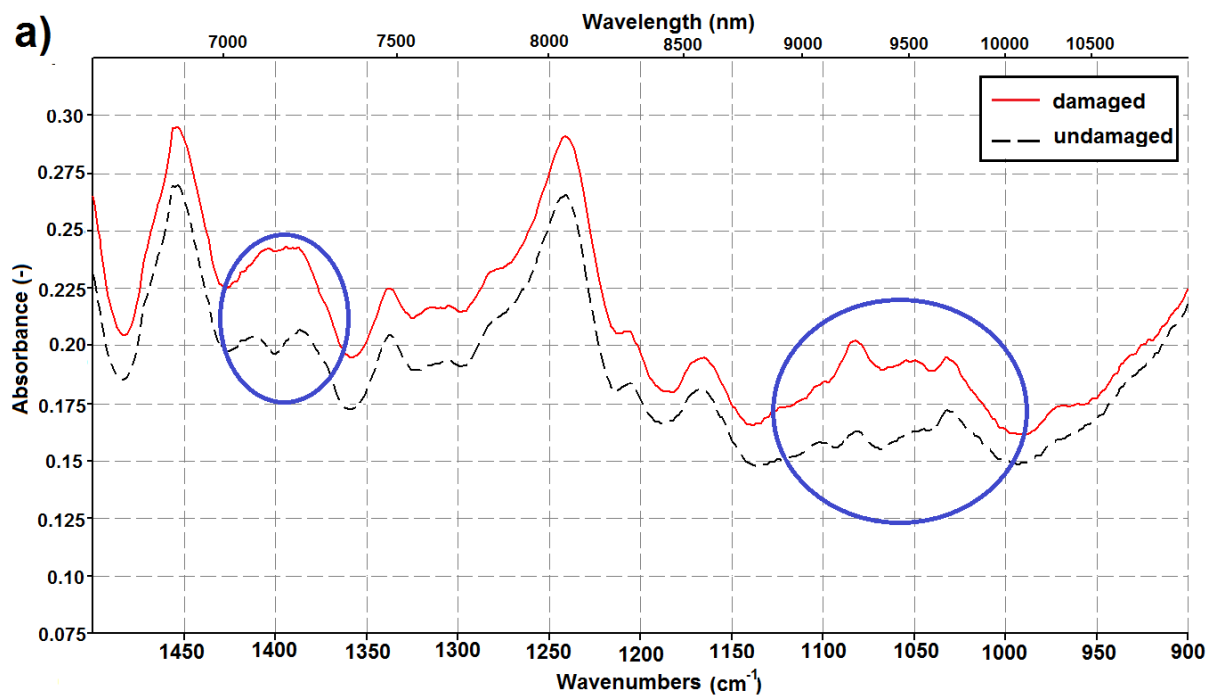
1. After damaging the tissue specimen with a catheter tip, it was transferred to a PBS-filled petri dish before being placed in a thermally insulated storage container for transport to the spectroscopy lab for ATR-FTIR analysis. All FTIR analyses were performed within thirty minutes of the tribological test.
2. Before analyzing the tissue specimen in the ATR-FTIR setup it was removed from the storage container and allowed to dry out for 3 to 5 minutes until the fluid film on the surface of the tissue had evaporated.
3. The ATR crystal and steel pressure cone were then cleaned using isopropanol. This was then followed by a waiting period of 30 s to ensure that the isopropanol had evaporated, before gently cleaning the ATR crystal and pressure cone with PBS.
4. The specimen was then placed over the ATR crystal using tweezers, taking care to ensure that the damaged part of the tissue was located correctly on the crystal.
5. The applied pressure of the ATR pressure cone on the specimen was adjusted using the 'live mode' to obtain a comparable overall absorption level in all tests, i.e., to ensure repeatability. This was accomplished by ensuring that the IR absorption intensity of the Amide II band (near 1400  $\text{cm}^{-1}$ ) had a value of 0.09 in each test.
6. After a short stabilization period of about 5 s, FTIR spectroscopic analysis was performed over a fixed integration time of 237 s (192 scans). Three scans were acquired for each specimen, from different locations, to confirm that the spectra obtained were repeatable.

## 4. RESULTS AND DISCUSSION

### 4.1 Spectroscopic analysis of qualitatively damaged ex-vivo aortic tissue

In **Figure 4a** major peaks are observed in both the damaged and fresh (i.e., undamaged) tissue IR spectra near  $1240\text{ cm}^{-1}$ ,  $1340\text{ cm}^{-1}$  and  $1460\text{ cm}^{-1}$ . Differences between fresh and damaged tissue can be seen in the wavenumber range between  $1000\text{ cm}^{-1}$  and  $1130\text{ cm}^{-1}$  (Region I), as well as between  $1360\text{ cm}^{-1}$  and  $1430\text{ cm}^{-1}$  (Region IV). Damage to the tissue causes the valley in Region IV to become shallower while the peaks in Region I (referred to hereafter as the ‘batman’ region) to become raised and more upright (**Figure 4**).

**Figure 4b and 4c** present close-up views of the wavenumber ranges corresponding to Region I and Region IV, showing that increasing tissue damage is associated with significant spectral changes in these regions. In the case of Region I shown in **Figure 4b** the spectral change with increasing tissue damage is a change in the orientation of the peak – which becomes raised and more upright with increasing tissue damage. In the case of Region IV greater shallowness of the valley between the peaks centered near  $1375\text{ cm}^{-1}$  and  $1425\text{ cm}^{-1}$  gradually occurs, with the spectra for longer abrasion times with the soft brush ( $\geq 480\text{ s}$ ) more similar to the spectrum for hard brush-treated tissue, while spectra for shorter soft-brush abrasion times ( $<480\text{ s}$ ) are more similar to undamaged tissue (i.e., with a steep valley between the  $1375\text{ cm}^{-1}$  and  $1425\text{ cm}^{-1}$  peaks).



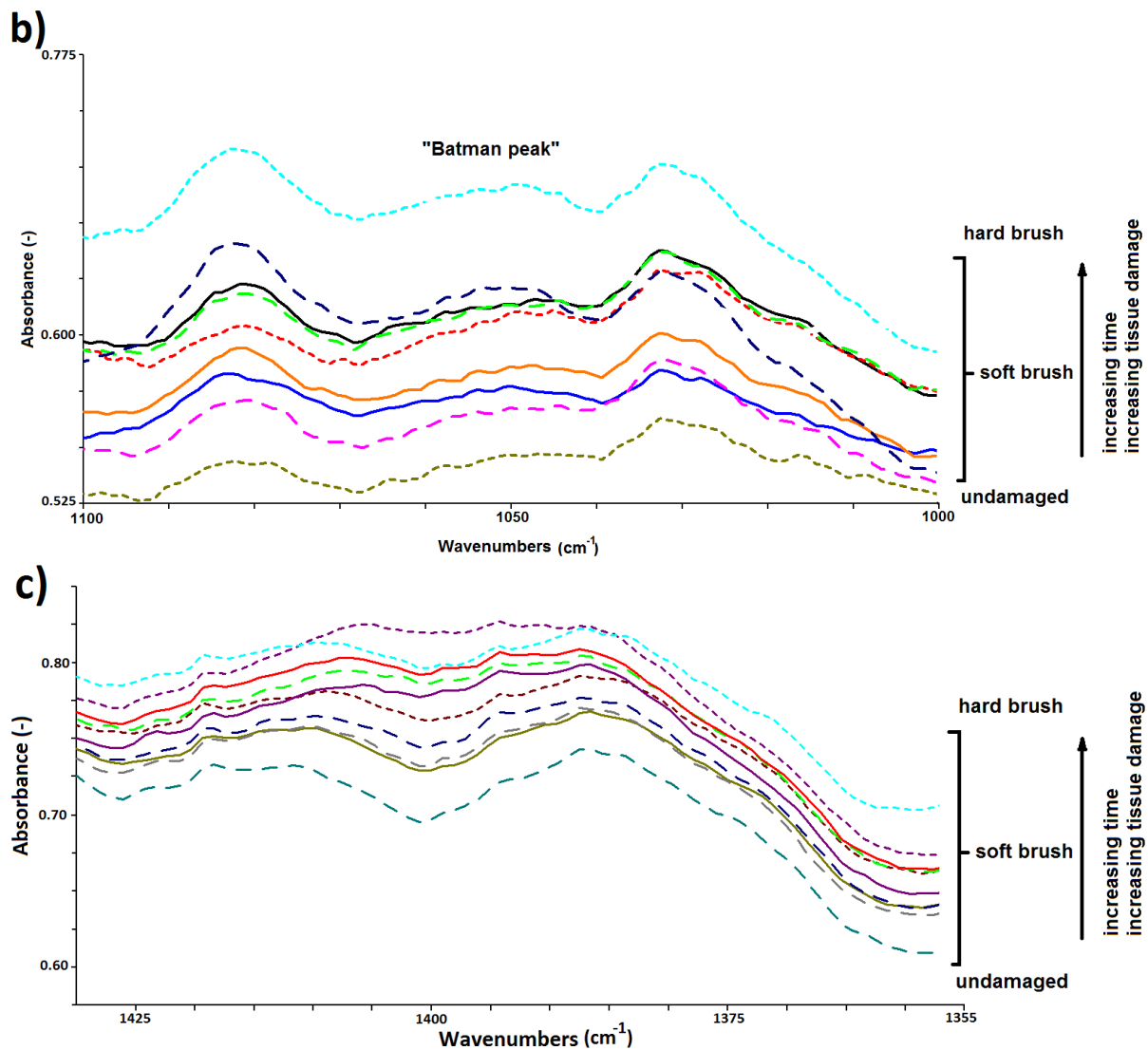


**Figure 4.** (a) Corrected and scaled IR absorption spectra for severely damaged (hard brush-treated) and undamaged ex-vivo porcine aortic tissue. Zoomed view of the corrected and scale IR absorption spectra highlighting the influence of increasing tissue damage from an undamaged to severely damaged (hard brush-treated) state, in: (b) Region I (1130-1000 cm<sup>-1</sup>) and (c) Region IV (1430-1360 cm<sup>-1</sup>).

A detailed summary of the observed spectral changes as the ex-vivo porcine aortic tissue is progressively damaged via abrasion, from an undamaged to a severely damaged state, is presented below in **Table 4**. The results reveal several interesting insights into tissue damage and highlight the sensitivity of IR spectroscopy to small differences in the chemical structure of the tissue (surface) due to mechanical damage. Gradual abrasion by the soft brush is already sufficient to induce progressive and distinctive changes in the IR absorption spectra. Most noticeably new peaks emerge near 1050 cm<sup>-1</sup> after 720s of abrasion, and disappear near 1102 cm<sup>-1</sup> and 1206 cm<sup>-1</sup> after 900 s of soft-brush abrasion. There is also a major peak shift 1387 cm<sup>-1</sup> to 1394 cm<sup>-1</sup> when tissue damage is further increased from 900 s of abrasion with the soft brush to damage from the hard one. Finally, it is interesting to note

that there are also small shifts in other peaks which arise as the tissue is progressively damaged by abrasion with the soft brush, including the peaks near 1081 cm<sup>-1</sup>, 1032 cm<sup>-1</sup>, 1167 cm<sup>-1</sup> and 1337 cm<sup>-1</sup>.

It is important to note here that these changes are likely linked to a wear process in which subsequent layers of tissue are gradually removed, revealing the chemical gradients within the tissue which produce the spectral changes observed. These results suggest that IR absorption spectroscopy is sufficiently sensitive to chemical changes in the aortic-tissue surface which occur when it is damaged and can be used to effectively assess the degree of damage to the tissue.

**Table 4 Peak listing for ex-vivo porcine aortic tissue progressively damaged using abrasion over controlled time intervals.**

Damage level Peak #	Undamaged	Soft brush (120 s)	Soft brush (240 s)	Soft brush (480 s)	Soft brush (720 s)	Soft brush (900 s)	Hard brush (15 s)	
1	1634.4	1634.4	1636.3	1634.4	1634.4	1634.4	1634.4	(cm <sup>-1</sup> )
2	1544.7	1545.7	1545.7	1545.7	1544.7	1544.7	1544.7	(cm <sup>-1</sup> )
3	1454.1	1456.0	1456.0	1456.0	1453.1	1456.0	1454.1	(cm <sup>-1</sup> )
4	1410.7	1410.7	1409.7	1410.7	1409.7	1407.8	-	(cm <sup>-1</sup> )
5	1386.6	1387.5	1387.5	1387.5	1387.5	1387.5	1394.3	(cm <sup>-1</sup> )
6	1337.4	1336.4	1338.4	1336.4	1337.4	1336.4	1336.4	(cm <sup>-1</sup> )
7	1305.6	1305.6	1305.6	1305.6	1306.5	1306.5	1305.6	(cm <sup>-1</sup> )
8	1241.0	1241.0	1241.9	1241.9	1241.9	1241.0	1241.0	(cm <sup>-1</sup> )
9	1206.3	1206.3	1205.3	1206.3	1206.3	-	-	(cm <sup>-1</sup> )
10	1167.7	1165.8	1166.7	1165.8	1166.7	1166.7	1164.8	(cm <sup>-1</sup> )
11	1102.1	1102.1	1102.1	1102.1	1103.1	-	-	(cm <sup>-1</sup> )
12	1080.9	1080.9	1081.9	1081.9	1080.9	1081.9	1082.8	(cm <sup>-1</sup> )
13	-	-	-	-	1048.1	1050.1	1050.1	(cm <sup>-1</sup> )
14	1031.7	1031.7	1031.7	1030.8 <sup>†</sup>	1032.7	1032.7	1032.7	(cm <sup>-1</sup> )

Legend: - = nil (i.e., no peak present), no peak shift, minor peak or vibrational shift and major peak shift.

#### 4.2 Spectroscopic analysis of controlled tribological damage to ex-vivo aortic tissue

**Figure 5** shows an example of the result of a controlled tissue damage test on the ex-vivo porcine aorta tissue using a catheter tip. It is possible to visually distinguish between the undamaged and damaged tissue surface, which has a damaged internal lamina membrane.

In practice, since the aortic tissue is extremely tough and resistant to piercing, it was found that abrasion (i.e., rubbing) of the catheter tip on the tissue did not lead to tearing of the tissue but only to the removal of the surface intima layer and the intima-media lamina, ultimately reaching the media layer. This may be attributed to the fairly small magnitude normal force applied (0.2 N) to the catheter tip, the angle of orientation of the catheter tip to the tissue as well as the stiffness of the catheter tip and shaft.

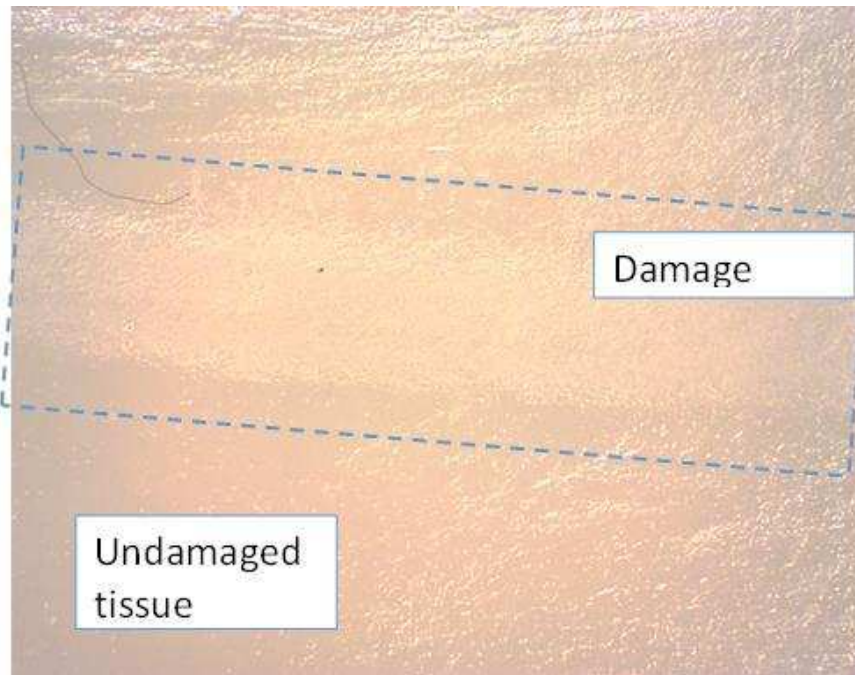


**Figure 5.** Image of ex-vivo porcine aorta tissue showing a damage track produced after CETR testing with 4 N normal force, 70° angle and with a free catheter tip length of 10 mm (magnification x6.3).

**Figure 6a** shows a comparison of the results obtained from undamaged tissue with the tissue damage experiments using catheter tip 1. From the figure it can be seen that one pass causes very little change in the spectrum, with the most visible changes occurring in the 1250-1350  $\text{cm}^{-1}$  wavenumber range (i.e., Region III) and near the peak at 1170  $\text{cm}^{-1}$  (Region II). After 1 pass only a very limited amount of material has been removed from the surface of the tissue. After 5 passes, the spectrum for the damaged region of porcine aorta is significantly altered and remains the same until 10 drags. It is likely that the damage between these two states occurs in the same layer.

**Figure 6b** shows the results obtained for the tissue damage experiments performed using catheter tip 2 (with reinforced steel wire), which causes greater stress to the tissue than catheter tip 1. The figure shows that significant spectral changes are visible at 1400  $\text{cm}^{-1}$  (Region IV), 1250-1350  $\text{cm}^{-1}$  (Region III), 1220  $\text{cm}^{-1}$ , 1170  $\text{cm}^{-1}$  (Region II) and 1080  $\text{cm}^{-1}$  (Region I). A single pass is sufficient to rub off the top material and reveal the underlying material. The observed changes are significant when compared to those observed for the

soft-brush experiments, with the compositional changes in the outermost layer of the aortic tissue being much more pronounced.

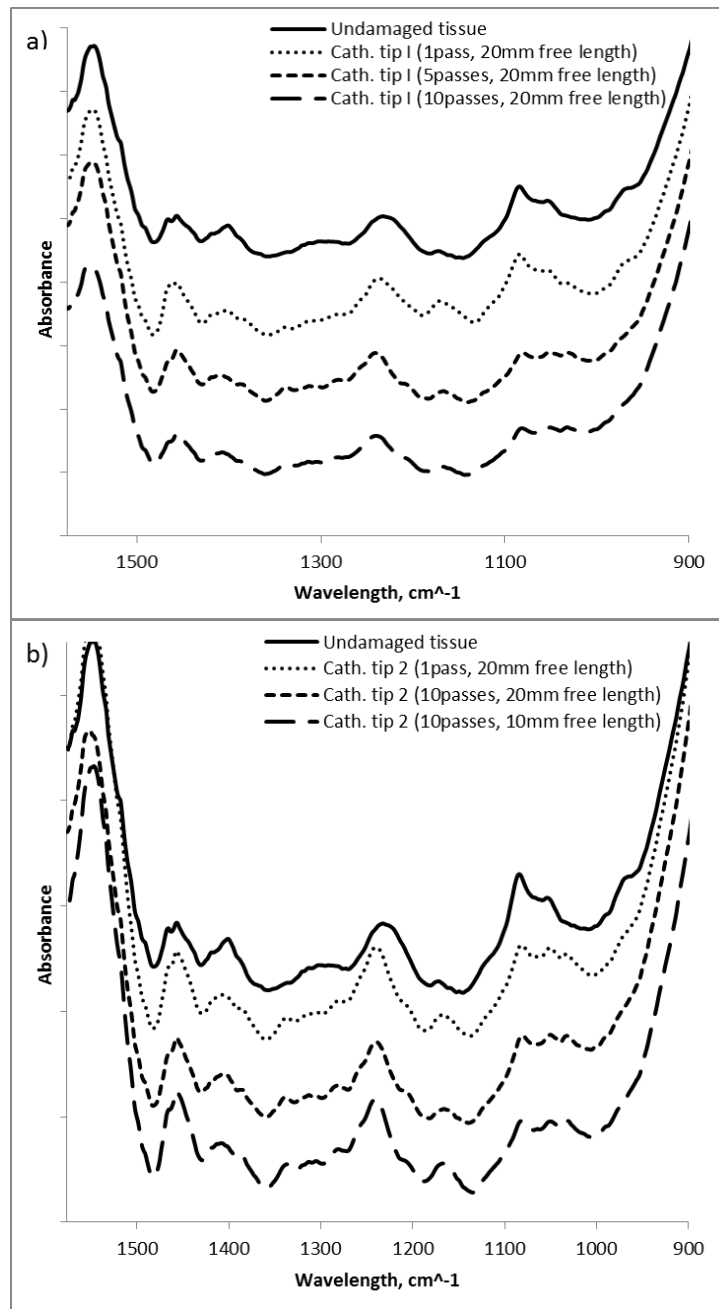


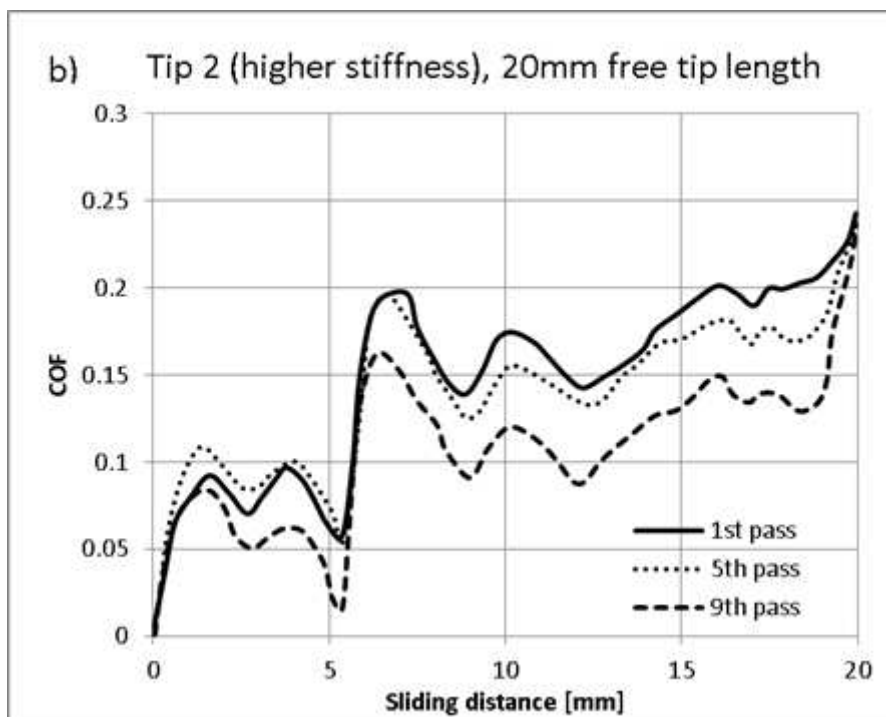
**Figure 6.** Scaled and corrected IR absorption spectra for undamaged and damaged ex-vivo porcine aortic tissue using: (a) Catheter tip 1: the damage state was achieved using the UMT with 0.2N normal force, 20mm free catheter tip length and a catheter orientation angle of 45° with respect to tissue. (b) Catheter tip 2: the damage state was achieved using the UMT with 0.2N normal force and a catheter orientation angle of 45° with respect to tissue. The catheter free catheter tip length was varied between 10 mm and 20 mm. Note that the vertical positions of the individual spectra have been shifted to avoid overlap and to more clearly highlight differences between spectra.

The degree of damage to the porcine aorta, as indicated by the FTIR results, is reflected in the observed COF for the different stiffness of catheter tip and number of passes. **Figure 7** shows the development of the COF for the lowest stiffness tip 1 (**Fig. 7a**), the stiffer tip 2 (**Fig. 7b**) and the stiffest tip 2 with shorter free tip length (**Fig. 7c**). In these figures, the COF

changes with sliding distance in an erratic manner but reproducible for each pass. The reproducibility indicates that the behaviour can be attributed to the uneven surface of the porcine aorta. The erratic changes in COF are due to variations in amount by which the catheter tip, which was oriented at 45° to the tissue, “digs in” to the tissue causing bow wave formation at the leading edge. This leads to variations in the ploughing or deformation component of the friction. For the lowest stiffness catheter tip (tip 1), the COF was approximately the same for all passes. Nevertheless, the FTIR results (**Figure 6a**) indicated significant spectral changes, so it is likely that the damage occurring between pass 1 and pass 9 is within the uppermost (intima) layer of the tissue. With the catheter tip of intermediate stiffness, **Figure 7b** shows that the friction decreased with increasing number of passes, and this is still more evident with the highest stiffness catheter tip (**Figure 7c**). The FTIR spectrum (**Figure 6b**) shows relatively large spectral changes as the catheter tip stiffness is increased, suggesting that these changes may be associated with greater tissue damage extending beyond the uppermost intima layer. Because it is known from tensile testing that the media is the softest of the three layers comprising the aortic tissue [52], it can be hypothesized that the reduction in COF with increasing surface damage may be attributed to a reduction in interfacial shear strength as the damage begins to extend from the intima into the media layer. This may lead to a reduction in the adhesion component of the friction which is given by:

$$F_{ADH} = \tau \cdot A_R \quad (2)$$

Where  $\tau$  is the interfacial shear strength [ $\text{N}\cdot\text{m}^{-2}$ ] and  $A_R$  is the real area of contact [ $\text{m}^2$ ].



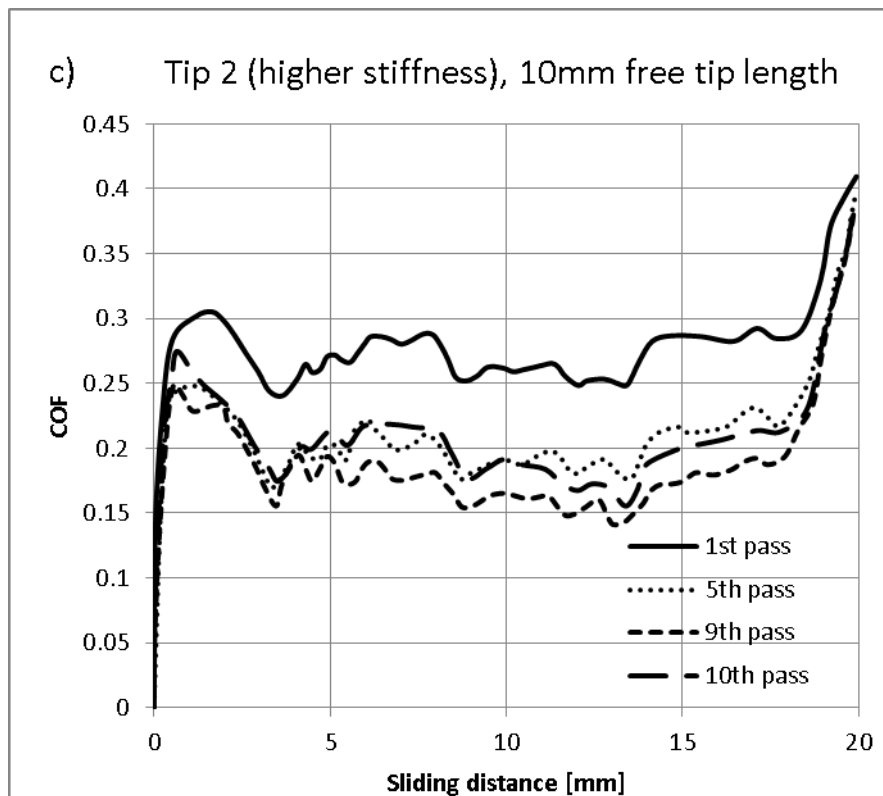


**Figure 7. Coefficient of friction for unidirectional passes as a function of time for: (a) catheter tip 1 with 20mm free tip length, passes 1, 5, 9 and 10; (b) catheter tip 2 with 20mm free tip length, passes 1, 5, and 9; (c) catheter tip 2 with 10mm free tip length, passes 1, 5, 9 and 10.**

These results clearly show that limited damage as induced with an actual catheter tip can be observed with ATR FTIR, provided the tissue is very carefully handled, and that the degree of damage shows some correlation with the friction coefficient. It is important to note that human blood vessel tissue, especially in the diseased condition, is likely to be more susceptible to damage than healthy porcine aorta, and may show differences under milder loading conditions. Additional tests on such material, correlated with histology, are required for a final confirmation of the suitability of FTIR for in-vivo catheter-induced damage and this will be addressed in future work.

## 5. CONCLUSIONS

ATR-FTIR spectroscopy was investigated as a method for the quantitative assessment of tissue damage during endovascular catheterization by performing qualitative and quantitative damage tests on ex-vivo porcine aortic tissue. ATR-FTIR spectroscopy has several key advantages over other spectroscopic approaches, since it is easy to perform and comparatively fast (a few minutes) as it has a high signal-to-noise ratio. Its sensitivity to polar functionalities enables easy detection of subtle differences in the biochemical structure of the various tissue-layers. As the application of ATR makes the method highly-surface specific analysis of the damaged tissue surface is possible. Based on the results obtained during the

tissue damage tests it can be concluded that FTIR spectroscopy is a reliable and effective measurement technique for quantifying tissue damage since it allowed very repeatable spectra to be obtained from the ex-vivo porcine aortic tissue for a period of up to 36 hours after excision, with no major spectral changes observed during this time frame due to tissue age (i.e., there were no differences observed between fresh and old tissue). Obvious changes were visible in the FTIR spectra as well as the friction coefficient as a function of increasing damage, even in the presence of small-scale tissue non-uniformity. In particular the spectral changes due to damage to the outermost layer of the aortic tissue were significant and suitable for analysis of realistic catheter-induced damage, provided appropriate sample conditioning is performed. The observed spectral changes that were associated with tissue damage and which correlated with a reduction in friction coefficient, can be attributed to the removal of successive layers of tissue with different chemical characteristics as a result of a 'wear process' (i.e., abrasion). With the experimental protocol applied here, it is unlikely that mechanical damage to the tissue produces biochemical changes that can be observed in FTIR spectra, since the aortic tissue has been removed from the body and does not contain blood.

#### **FUNDING ACKNOWLEDGMENT**

This work was supported by the European Commission Framework Programme 7 through grant FP7-PEOPLE-2011-IAPP/286174. Author JW would like to acknowledge the Polish Ministry of Science and Higher Education for financial support for the research within the co-financed international project in the years 2012-2016.

#### **ACKNOWLEDGMENTS**

The authors thank Hans Kroes for his help in the design and fabrication of the custom-built tissue and catheter tip holders.

#### **CONFLICT OF INTEREST**

The authors are unaware of any conflicts of interest.

#### **STATEMENT OF HUMAN STUDIES**

This study did not involve the use of human subjects. All data were obtained from surveying the published literature and from in vitro tests on ex-vivo porcine aortic tissue.

#### **STATEMENT OF ANIMAL STUDIES**

This study involved *in vitro* testing on ex-vivo porcine aortic which was sourced from Hemolab B.V., Eindhoven, the Netherlands, an ethical supplier of animal tissue. The tests were conducted with the approval and in accordance with the guidelines of the Philips Research Internal Committee for Biological Experiments.

## REFERENCES

1. Nichols M, Townsend N, Scarborough P, Rayner M. Cardiovascular disease in Europe 2014: epidemiological update. *Eur Heart J*. 2014; doi: 10.1093/eurheartj/ehu299
2. Moore WS, Ahn SS. *Endovascular surgery*. 4th ed. Philadelphia: Elsevier Saunders; 2011.
3. Ratner BD. The catastrophe revisited: blood compatibility in the 21st century. *Biomaterials*. 2007; doi: 10.1016/j.biomaterials.2007.07.035
4. Aggarwal A, Dai D, Rumsfeld JS, et al. Incidence and predictors of stroke associated with percutaneous coronary intervention. *Am J Cardiol*. 2009; doi: 10.1016/j.amjcard.2009.03.046
5. Genereux P, Webb JG, Svensson LG, et al. Vascular complications after transcatheter aortic valve replacement: insights from the PARTNER trial. *J Am Coll Cardiol*. 2012; doi: 10.1016/j.jacc.2012.07.003
6. Jia DA, Zhou YJ, Shi DM, et al. Incidence and predictors of radial artery spasm during transradial coronary angiography and intervention. *Chin Med J*. 2010 doi: 10.3760/cma.j.issn.0366-6999.2010.07.015
7. Dellimore KH, Franklin SE, Helyer A. A review of catheter related complications during minimally invasive transcatheter cardiovascular intervention with implications for catheter design. *Cardiovasc Eng Technol*. 2014; doi: 10.1007/s13239-014-0183-9
8. Sanborn TA, Haudenschild CC, Garber GR, Ryan TJ, Faxon DP. Angiographic and histologic consequences of laser thermal angioplasty: comparison with balloon angioplasty. *Circulation*. 1987; doi: 10.1161/01.CIR.75.6.1281
9. Rubin E, Reisner H. *Essentials of Rubin's pathology*. 5th ed. Baltimore: Lippincott Williams & Wilkins; 2009.
10. Guelinckx PJ, Boeckx WD, Fossion E, Gruwez JA. Scanning electron microscopy of irradiated recipient blood vessels in head and neck free flaps. *Plast Reconstr Surg*. 1984; doi: 10.1097/00006534-198408000-00008
11. Lamb FS, King CM, Harrell H, Burkel W, Webb RC. Free radical-mediated endothelial damage in blood vessels after electrical stimulation. *Am J Phys - Heart Circ Phys*. 1987;252(5):H1041-H1046.
12. Weston AE, Armer HEJ, Collins LM. Towards native-state imaging in biological context in the electron microscope. *J Chem Biol*. 2010; doi: 10.1007/s12154-009-0033-7

13. Hekking LH, Lebbink MN, Winter DA, et al. Focused ion beam-scanning electron microscope: exploring large volumes of atherosclerotic tissue. *J Microsc.* 2009; doi: 10.1111/j.1365-2818.2009.03274.x
14. Wong RC, Yazdanfar S, Izatt JA, et al. Visualization of subsurface blood vessels by color Doppler optical coherence tomography in rats: before and after hemostatic therapy. *Gastrointest Endosc.* 2002; doi: 10.1067/mge.2002.120104
15. Srinivasan VJ, Mandeville ET, Can A, et al. Multiparametric, longitudinal optical coherence tomography imaging reveals acute injury and chronic recovery in experimental ischemic stroke. *Plos One.* 2013; doi: 10.1371/journal.pone.0071478
16. Weiss L. Damage and death in tissues and associated changes in their mechanical properties. in *Ultrasonic tissue characterization II.* Linzer M ed. National Bureau of Standards. Spec. Publ. 525. Washington DC: U.S. Government Printing Office; 1979.
17. Accardi MA, McCullen SD, Callanan A, et al. Effects of fiber orientation on the frictional properties and damage of regenerative articular cartilage surfaces. *Tissue Eng Part A.* 2013; doi: 10.1089/ten.TEA.2012.0580
18. Hanlon EB, Manoharan R, Koo TW, et al. Prospects for in vivo Raman spectroscopy. *Phys Med Biol.* 2000; doi: 10.1088/0031-9155/45/2/201
19. Votteler M, Carvajal Berrio DA, Pudlas M, et al. Raman spectroscopy for the non-contact and non-destructive monitoring of collagen damage within tissues. *J Biophotonics.* 2012; doi: 10.1002/jbio.201100068
20. Bonnier F, Rubin S, Venteo L. In-vitro analysis of normal and aneurismal human ascending aortic tissues using FT-IR microspectroscopy. *Biochim Biophys Acta.* 2006; doi:10.1016/j.bbamem.2006.05.018
21. Cheheltani R, McGoverin C, Rao J, et al. Fourier transform infrared spectroscopy to quantify collagen and elastin in an in vitro model of extracellular matrix degradation in aorta. *Analyst.* 2014; doi: 10.1039/c3an02371k
22. Colley C, Kazarian S, Weinberg P. Spectroscopic imaging of arteries and atherosclerotic plaques. *Biopolymers.* 2004; doi: 10.1002/bip.20069
23. Chen YM, Kurokawa T, Tominaga T, et al. Study on the sliding friction of endothelial cells cultured on hydrogel and the role of glycocalyx on friction reduction. *Adv Eng Mater.* 2010; doi: 10.1002/adem.201080021
24. Sobolewski P, El Fray M. Cardiac catheterization: consequences for the endothelium and potential for nanomedicine. *WIREs Nanomed Nanobiotechnol.* 2015; doi: 10.1002/wnan.1316
25. Neviliappan S, Kan L, Walter T, Arulkumaran M. Infrared spectral features of exfoliated cervical cells, cervical adenocarcinoma tissue, and an adenocarcinoma cell line (SiSo). *Gynecol Oncol.* 2002; doi: 10.1006/gyno.2002.6602

26. Erukhimovitch V, Talyshinsky M, Souprun Y. FTIR spectroscopy examination of leukemia patients plasma. *Vib Spectrosc.* 2006; doi:10.1016/j.vibspec.2005.06.004
27. Gentner J, Wentrup-Byrne E, Walker P, Walsh M. Comparison of fresh and post-mortem human arterial tissue: An analysis using FT-IR microspectroscopy and chemometrics. *Cell Mol Biol.* 1998;1(44):251-9.
28. Schulz C, Liu K, Johnston J, Mantsch H. Study of chronic lymphocytic leukemia cells by FT-IR spectroscopy and cluster analysis. *Leuk Res.* 1996;20(8):649-55.
29. Parker F, Ans R. Infrared studies of human and other tissues by the attenuated total reflection technique. *Anal Biochem.* 1967; doi: 10.1016/0003-2697(67)90099-1
30. Manoharan R, Baraga JJ, Rava RP, et al. Biochemical analysis and mapping of atherosclerotic human artery using FT-IR microspectroscopy. *Atherosclerosis.* 1993; doi: 10.1016/0021-9150(93)90261-R
31. Lasch P, Boese M, Pacifico A, Diem M. FT-IR spectroscopic investigations of single cells on the subcellular level. *Vib Spectrosc.* 2002; doi: 10.1016/S0924-2031(01)00153-9
32. Palombo F, Cremens S, Weinberg P, Kazarian S. Application of Fourier transform infrared spectroscopic imaging to the study of effects of age and dietary L-arginine on aortic lesion composition in cholesterol-fed rabbits. *J R Soc Interface.* 2009; doi: 10.1098/rsif.2008.0325
33. Aning J. Critique of fourier transform infrared microspectroscopy applications to prostate pathology diagnosis. Ph.D. Dissertation. Cranfield University, Cranfield UK; 2010.
34. Chalmers J, Griffiths P. *Handbook of vibrational spectroscopy.* 5th ed. Chichester: Wiley & Sons Ltd.; 2002.
35. Chiriboga L, Xie P, Yee H, et al. Infrared spectroscopy of human tissue. I. Differentiation and maturation of epithelial cells in the human cervix. *Biospectroscopy.* 1998; doi: 10.1002/(SICI)1520-6343
36. Lin S, Li M, Cheng W. FT-IR and Raman vibrational microspectroscopies used for spectral biodiagnosis of human tissues. *Spectroscopy.* 2007;21:1-30.
37. Rubin S, Bonnier F, Sandt C, et al. Analysis of structural changes in normal and aneurisal human aortic tissues using FTIR microscopy. *Biopolymers.* 2007; doi: 10.1002/bip.20882.
38. Dukor RK. Vibrational spectroscopy in the detection of cancer. in *Handbook of vibrational spectroscopy*, eds. J. M. Chalmers and P. R. Griffiths. Chichester: John Wiley and Sons Ltd.; 2006.

39. Wrobel T, Marzec K, Majzner K, et al. Attenuated total reflection Fourier transform infrared (ATR-FTIR) spectroscopy of a single endothelial cell. *Analyst*. 2012; doi: 10.1039/c2an35331h
40. Mirabella F, Internal reflection spectroscopy: Theory and applications. 15<sup>th</sup> ed. New York: Marcel Dekker Inc.; 1993.
41. Morent R, De Geyter N. Improved textile functionality through surface modifications,” in *Functional textiles for improved performance, protection and health*. 15<sup>th</sup> ed. Philadelphia: Woodhead Publishing; 2011.
42. Oelichmann J. Surface and depth-profile analysis using FTIR spectroscopy. *Fresen Z Anal Chem*. 1989; doi: 10.1007/BF00572327
43. Pike Technologies. ATR - Theory and applications. Application note. Madison WI, USA; 2011.
44. Feng D. Modelling and control in biomedical systems. 1st ed. London: Elsevier; 2006.
45. Meer FV. Vascular applications of quantitative optical coherence tomography. PhD. Dissertation, University of Amsterdam, Amsterdam; 2005.
46. Dirckx J, Kuypers L, Decraemer W. Refractive index of tissue measured with confocal microscopy. *J Biomed Opt*. 2005; doi: 10.1117/1.1993487
47. Niemczyk A, El Fray M, Franklin SE. Friction behaviour of hydrophilic lubricious coatings for medical device applications. *Tribol Int*. 2015; doi: 10.1016/j.triboint.2015.02.003
48. Xiao N, Guo J, Guo S, Tamiya T. A robotic catheter system with real-time force feedback and monitor. *Australas Phys Eng Sci Med*. 2012; doi: 10.1007/s13246-012-0146-0
49. Yokoyama K, Nakagawa H, Shah DC, et al. Novel contact force sensor incorporated in irrigated radiofrequency ablation catheter predicts lesion size and incidence of steam pop and thrombus. *Circulation*. 2008; doi: 10.1161/CIRCEP.108.803650
50. Schoemaker I. Forces during in vivo manipulations of catheters. MSc. Thesis Technical Universiteit Delft, Delft; 2008.
51. Dunn A, Saveri TD, Keselowsky BG, Sawyer WG. Macroscopic friction coefficient measurements on living endothelial cells. *Tribol Lett*. 2007; doi: 10.1007/s11249-007-9230-0.
52. Holzapfel G.A., Schulze–Bauer C.A.J., Stadler M. in: J. Casey, and G. Bao, eds., *Mechanics in Biology*, AMD-Vol. 242, BED-Vol. 46, New York (2000), 141-156.